

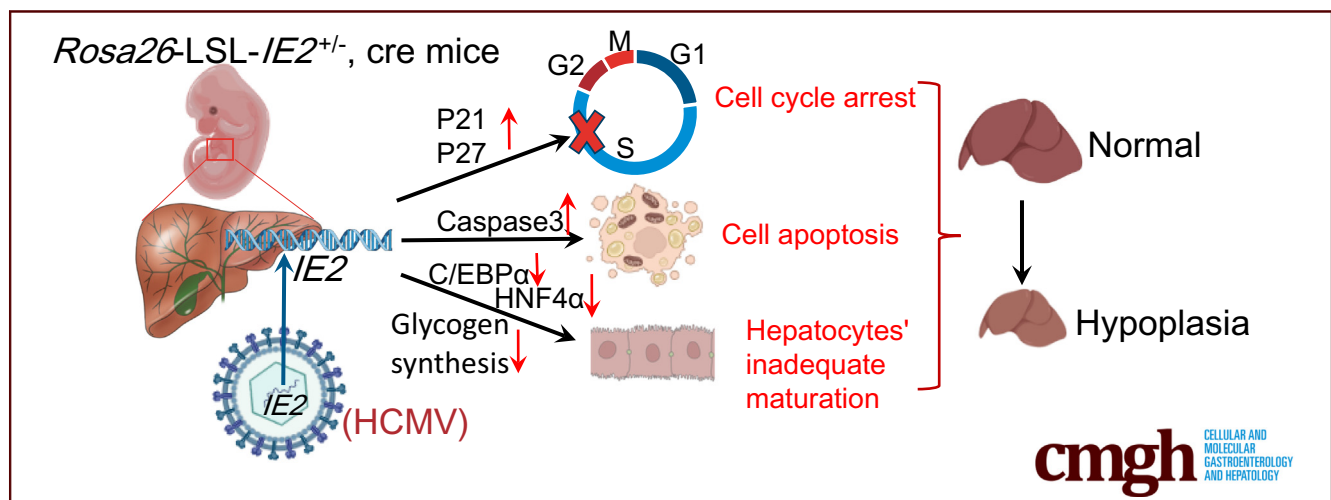
ORIGINAL RESEARCH

Human Cytomegalovirus-IE2 Affects Embryonic Liver Development and Survival in Transgenic Mouse



Xianjuan Zhang,^{1,*} Shasha Jiang,^{1,*} Xiaoqiong Zhou,¹ Zhongjie Yu,² Shuo Han,^{3,4} Fulong Nan,² Hongye Qiao,¹ Delei Niu,¹ Zhifei Wang,¹ Junyun Niu,¹ Hong Zhang,⁵ Ting Liu,⁶ Yunyang Wang,^{7,§} and Bin Wang^{1,2,§}

¹Department of Pathogenic Biology, School of Basic Medicine, Qingdao University, Qingdao, China; ²Department of Special Medicine, School of Basic Medicine, Qingdao University, Qingdao, China; ³Department of Spinal Surgery, Affiliated Hospital of Qingdao University, Qingdao, China; ⁴Department of Medicine, Qingdao University, Qingdao, China; ⁵School of Public Health, Qingdao University, Qingdao, China; ⁶Qingdao Municipal Hospital, Qingdao, China; and ⁷Department of Endocrinology and Metabolism, Affiliated Hospital of Qingdao University, Qingdao, China



SUMMARY

In this study, a transgenic mouse model that could specifically and stably express the immediate-early protein 2 (IE2) in the liver was constructed to simulate the pathology of the effect of IE2 expression on cells after human cytomegalovirus infection. Results showed that a consistent IE2 expression affects the orderly process of embryonic liver development by disrupting hepatic morphogenesis and hepatocyte maturation, resulting in lethality at embryonic day 17.5 to day 1.

BACKGROUND & AIMS: Congenital human cytomegalovirus (HCMV) infection is a common cause of liver injury. The major immediate-early protein 2 (IE2) of HCMV is critical for the progression of HCMV infection. As a result of species isolation, there are no animal models suitable for HCMV infection, which aimed to study the long-term effects of IE2 on embryonic liver development in vivo. Hence, this study aimed to investigate the role of IE2 in liver development using a transgenesis mouse model.

METHODS: *Rosa26-Loxp-STOP-Loxp (LAS)-IE2^{+/-}*, cre mice that could specifically and stably express IE2 in the liver, were constructed. Phenotypic analysis, immunolocalization studies,

messenger RNA analyses, transcriptome sequencing, and flow cytometry analysis were performed on *Rosa26-LSL-IE2^{+/-}*, cre mice during hepatogenesis.

RESULTS: *Rosa26-LSL-IE2^{+/-}*, cre mice could consistently express IE2 at different embryonic stages in vivo. With the development of *Rosa26-LSL-IE2^{+/-}*, cre embryos from embryonic day 17.5 to postnatal day 1, progressive liver hypoplasia and embryonic deaths were observed. Furthermore, molecular evidence that IE2 expression inhibited hepatocyte proliferation, increased cell apoptosis, and impaired hepatocyte maturation was provided.

CONCLUSIONS: *Rosa26-LSL-IE2^{+/-}*, cre mice could stably express IE2 in the liver. IE2 expression resulted in embryonic liver hypoplasia by disrupting hepatic morphogenesis and hepatocyte maturation, which may be responsible for embryonic deaths. This study is helpful in understanding the mechanism of liver injuries induced by HCMV infection. (*Cell Mol Gastroenterol Hepatol* 2022;14:494–511; <https://doi.org/10.1016/j.jcmgh.2022.05.002>)

Keywords: Human Cytomegalovirus; IE2; Liver Development; Mouse Model.

Human cytomegalovirus (HCMV), a member of the β -herpesviruses, is the most common virus that causes congenital infection, affecting 0.4%–1% of live births.¹ HCMV infection is a major cause of birth defects including liver injury, hearing and visual loss, neurologic deficits, and intrauterine growth retardation, and may contribute to adverse consequences such as stillbirth and premature delivery.^{2–7} The clinical manifestations of liver injury induced by congenital HCMV infection vary, including hepatomegaly, hepatitis, cholestatic hepatopathy, and cirrhosis.^{8–10} Because liver structure and function are critical for circulation, metabolism, and nutrition, liver injuries caused by HCMV infection should be taken seriously. As a result of the strict species-specific tropism of HCMV, an animal model of HCMV infection has not been established yet. Hence, the *in vivo* mechanism of liver injuries caused by HCMV remains unclear.

Immediate-early protein 2 (IE2), a 579-amino acid protein, is encoded by the immediate-early gene *IE2*. As a master transcriptional regulator, IE2 could induce the expression of other virus-related genes and independently regulate host cell promoters.^{11,12} The perturbation of cell growth control by IE2 may be one of the ways in which virus promotes the development of some diseases, such as mental retardation and microcephaly.^{13,14} However, the effects of HCMV-IE2 on liver development are unclear, and further research is needed to elucidate the specific effects and mechanisms involved.

In this study, a transgenesis mouse *Rosa26-Loxp-STOP-Loxp (LSL)-IE2^{+/-}*, cre that could specifically and stably express IE2 in the liver was established. The long-term effects of IE2 on the liver and their underlying mechanisms were investigated *in vivo*. The results suggest that IE2 expression in the liver has a negative impact on hepatic morphogenesis and hepatocyte maturation during hepatogenesis. Moreover, IE2 accumulation resulted in late embryonic lethality. This study provides a new insight on the underlying mechanisms of molecular pathogenesis through which HCMV induces liver damage.

Results

Liver Hypoplasia and Late Embryonic Lethality Were Observed in IE2-Expressing Mice

To explore the effects of IE2 on the liver, a transgenic mouse model (*Rosa26-LSL-IE2^{+/-}*, cre) that could long-term stably express IE2 in the liver was constructed. *Rosa26-LSL-IE2^{+/-}*, cre mice were genotyped by polymerase chain reaction (PCR) and further confirmed by Western blot (Figure 1A and B). Surprisingly, among 88 neonatal mice, no live *Rosa26-LSL-IE2^{+/-}*, cre mice were obtained. Embryonic lethality occurred between embryonic day (E)17.5 and day (D)1 (Table 1).

Consistent with this lethality, in *Rosa26-LSL-IE2^{+/-}*, cre mice, the whole liver became smaller, with lower liver weight and liver/body weight ratio at E17.5–D1 compared with those of control embryos (*Rosa26-LSL-IE2^{+/-}*) (Figure 1C and D). The histologic staining of liver tissue sections showed that the red blood cells were nearly all anucleated at hepatic vessels, and hepatocytes were

beginning to organize and form mature hepatic cords from E17.5 in control embryos. However, *Rosa26-LSL-IE2^{+/-}*, cre embryos showed an abnormal architecture; at E17.5, the cellularity of the liver was reduced, and the empty space was increased; by D1, the liver structure was disordered, with large necrotic areas and irregularly arranged hepatocytes. Meanwhile, abundant nucleated red blood cells were observed in the liver and cardiac cavity (Figure 1E).


Then, IE2 expression was detected in *Rosa26-LSL-IE2^{+/-}*, cre livers. As shown in Figure 1F, IE2 was expressed consistently at different embryonic stages E15.5, E17.5, and D1, while it was strongly expressed from E17.5. All of these data indicate that the late lethality of *Rosa26-LSL-IE2^{+/-}*, cre embryos was probably linked to severe liver hypoplasia and phenotypic defects that may result from the strong activation of IE2 signaling at E17.5–D1, which is a critical period for liver morphogenetic and metabolic development.

Loss of Hepatoblasts and Hepatocytes in IE2-Expressing Liver During Liver Development

The specific expression of albumin (ALB) in hepatoblasts and hepatocytes¹⁵ led to the activation of *IE2* transcription and translation processes in both cells of our mouse model. To understand the causes of the abnormal liver architecture in *Rosa26-LSL-IE2^{+/-}*, cre mice at the cellular level, the numbers of hepatoblasts and hepatocytes were measured by α -fetoprotein (AFP)/ δ -like non-canonical notch ligand 1 (DLK1) and ALB immunostaining, respectively (Figure 2A and B). AFP and DLK1 are established hepatoblast markers, whereas ALB is a hepatocyte marker. Overall, DLK1- and AFP-positive cells were decreased continuously, while ALB-positive cells were increased gradually in 2 groups with liver development, but the expression levels in the 2 groups were significantly different at the same stage. Specifically, at E15.5, there was no significant difference in DLK1-, AFP-, and ALB-positive cells between the 2 groups, whereas at E17.5, DLK1-, AFP-, and ALB-positive cells were significantly lower than those in the control group. By D1, DLK1- and AFP-positive cells almost disappeared in the control group, but still existed in the IE2-expressing group. ALB-positive cells were dramatically lower in the IE2-expressing group than

*Authors share co-first authorship; [§]Authors share co-corresponding authorship.

Abbreviations used in this paper: AFP, α -fetoprotein; ALB, albumin; C/EBP α , CCAAT/enhancer binding protein alpha; CRISPR/Cas9, clustered regularly interspaced shortpalindromic repeats /CRISPR-associated 9; D, day; DEG, differentially expressed gene; DLK1, δ -like non-canonical notch ligand 1; E, embryonic; GO, Gene Ontology; GSEA, gene set enrichment analysis; HCMV, human cytomegalovirus; HNF4 α , hepatic nuclear factor 4 α ; IE2, immediate-early protein 2; KEGG, Kyoto Encyclopedia of Genes and Genomes; LSL, Loxp-STOP-Loxp; mRNA, messenger RNA; PCR, polymerase chain reaction; PPI, protein–protein interaction; TNF, tumor necrosis factor.

 Most current article

© 2022 The Authors. Published by Elsevier Inc. on behalf of the AGA Institute. This is an open access article under the CC BY-NC-ND license (<http://creativecommons.org/licenses/by-nc-nd/4.0/>).

2352-345X

<https://doi.org/10.1016/j.jcmgh.2022.05.002>

in the control group. Because IE2 expression was significantly higher at E17.5–D1 than at E15, a small amount of IE2 expression had no significant effect on the number of

hepatoblasts and hepatocytes, but its long-term and strong expression might disrupt liver morphogenesis by affecting the number of hepatoblasts and hepatocytes.

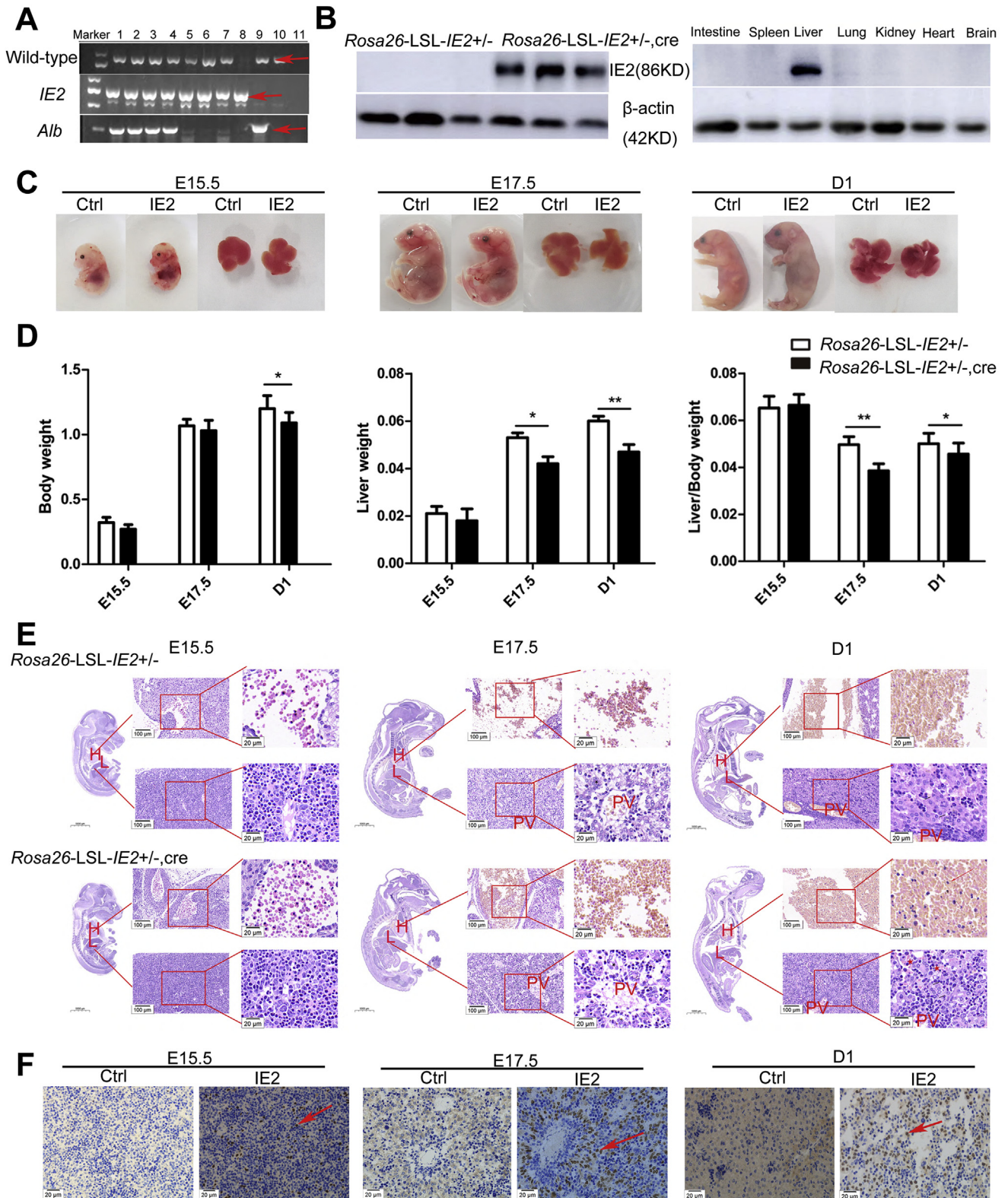


Table 1. Genotypes and Survival Status of Mice Resulting From *Rosa26-LSL-IE2^{+/-}* Crosses With Albumin-Cre Mice

Genotype	<i>Rosa26-LSL-IE2^{+/-}</i> , cre (survival)	<i>Rosa26-LSL-IE2^{+/-}</i> (survival)	<i>Rosa26-LSL-IE2^{-/-}</i> , cre (survival)	<i>Rosa26-LSL-IE2^{-/-}</i> (survival)	Total
Stage					
E15.5	6 (live)	11 (live)	14 (live)	12 (live)	44
E17.5	5 (live)	9 (live)	10 (live)	11 (live)	36
D1	19 (dead)	19 (live); 2 (dead)	32 (live); 3 (dead)	13 (live)	88

A Dramatic Alteration in Gene Expression in *IE2*-Expressing Liver

To rule out the possibility that clustered regularly interspaced shortpalindromic repeats/CRISPR-associated 9 (CRISPR/Cas9) technology exerted a negative influence on liver development and to further explore the molecular mechanism of liver injury caused by *IE2* expression, total RNA was isolated from the livers of D1 *Rosa26-LSL-IE2^{+/-}* mice, wild-type mice, and *Rosa26-LSL-IE2^{+/-}*, cre mice for transcriptome sequencing. A total of 6 Gb of data per sample were obtained, and the average data quality 30 (Q30) was greater than 93%, which indicates that the results of the RNA-sequencing analyses were reliable (Table 2). Correlation and principal component analyses indicated that the gene expression patterns of *Rosa26-LSL-IE2^{+/-}* mice were highly similar to those of wild-type mice, but were significantly different from those of *Rosa26-LSL-IE2^{+/-}*, cre mice (Figure 3A and B). In addition, genomic region distribution analysis showed that the proportions of the 3' untranslated region (3' UTR) and coding sequence (CDS) expression were significantly increased and decreased, respectively, in *Rosa26-LSL-IE2^{+/-}*, cre mice (Figure 3C). These data showed that the CRISPR/Cas9 technology used to construct the *Rosa26-LSL-IE2^{+/-}* mouse model did not affect the liver, while the liver transcriptome alterations may be attributed to the specific expression of *IE2*.

Then, differentially expressed genes (DEGs) were analyzed by edgeR packages of R (<https://www.r-project.org/>, Supplementary Table 1). In total, 3723 genes were expressed differentially (1717 genes were up-regulated, and 2006 genes were down-regulated) in the *Rosa26-LSL-IE2^{+/-}*, cre group compared with those in the *Rosa26-LSL-IE2^{+/-}* group (Figure 3D and E). DEGs were identified based on an adjusted *P* value less than .05 and absolute value of log₂ fold change greater than 1. The differences in the expression of top DEGs in the 2 groups were verified by quantitative real-time PCR (Figure 3F).

IE2-Specific Expression Affects Multiple Steps of Liver Development In Vivo

To further verify the effect of *IE2* expression on the liver in vivo, Gene Ontology (GO) and Kyoto Encyclopedia of Genes and Genomes (KEGG) enrichment were performed to analyze the biological functions of the DEGs. KEGG analysis showed that the up-regulated genes were enriched mainly in herpes simplex infection, cell cycle, and apoptosis (Figure 4A, Supplementary Table 2), while the down-regulated genes were enriched significantly in metabolic pathways, chemical carcinogenesis, complement and coagulation cascades, and fatty acid degradation (Figure 4C, Supplementary Table 3). GO analysis showed that the enriched categories of up-regulated genes were associated mainly with DNA replication, including nucleosome assembly, DNA packaging, nucleosome organization, and chromatin assembly (Figure 4B, Supplementary Table 4). However, the enriched categories of down-regulated genes were related mainly to hepatocyte functions, including metabolic and oxidation reduction processes (Figure 4D, Supplementary Table 5).

Based on the string protein interaction database (<http://StringDB.org>), a protein-protein interaction (PPI) network was used to illustrate the interaction among the DEGs of the *Rosa26-LSL-IE2^{+/-}*, cre group. By ranking their degrees, the top 30 hub regulatory genes in the PPI network were determined (Table 3). Interestingly, these hub DEGs with higher degrees were associated mainly with cell cycle (*Ccnb1*, *Ccna2*, *Jun*, and *Pcna*) and DNA damage (*Rad21* and *Bub1*), suggesting that the overall changes of the liver transcriptome in *Rosa26-LSL-IE2^{+/-}*, cre mice may be caused by abnormal cell proliferation and DNA damage response. Taken together, these results indicate that *IE2* affects multiple processes of liver development, including cell proliferation, apoptosis, liver metabolism, and liver synthetic function.

Failure of Proliferation in *IE2*-Expressing Liver

To further determine how *IE2* affects the cell-cycle progression, a network of cell-cycle-related genes was

Figure 1. (See previous page). Liver hypoplasia and death of embryos in *Rosa26-LSL-IE2^{+/-}*, cre mice. (A) *Rosa26-LSL-IE2^{+/-}*, cre mice were identified by PCR (red arrows). Lanes 1–4, *Rosa26-LSL-IE2^{+/-}*, cre mice; lanes 5–7, *Rosa26-LSL-IE2^{+/-}* mice; lane 8, homozygous *Rosa26-LSL-IE2^{+/-}* mice; lane 9, albumin-cre mice; lane 10, wild-type mice, and lane 11, the water control. PCR product size was as follows: *IE2*, 819 bp; *Alb*, 245 bp; and wild-type, 994 bp. (B) Specifically expressed *IE2* in *Rosa26-LSL-IE2^{+/-}* mice liver was confirmed by Western blot. (C) Morphology of whole embryos and livers of E15.5, E17.5, and D1. (D) Weight of body and liver and liver/body of E15.5, E17.5, and D1 embryos. (E) E15.5, E17.5, and D1 embryo sagittal sections stained with H&E. (F) *IE2* expression in the livers at stages E15.5, E17.5, and D1 were detected by immunohistochemical staining (red arrows). Scale bars: 20 μm. Ctrl represents *Rosa26-LSL-IE2^{+/-}*, and IE2 represents *Rosa26-LSL-IE2^{+/-}*, cre. Asterisks represent megakaryocytes. Error bars represent SEM. **P* < .05, ***P* < .01. n = 3–5 mice per group. Ctrl, control; H, heart; L, liver; PV, portal vein.

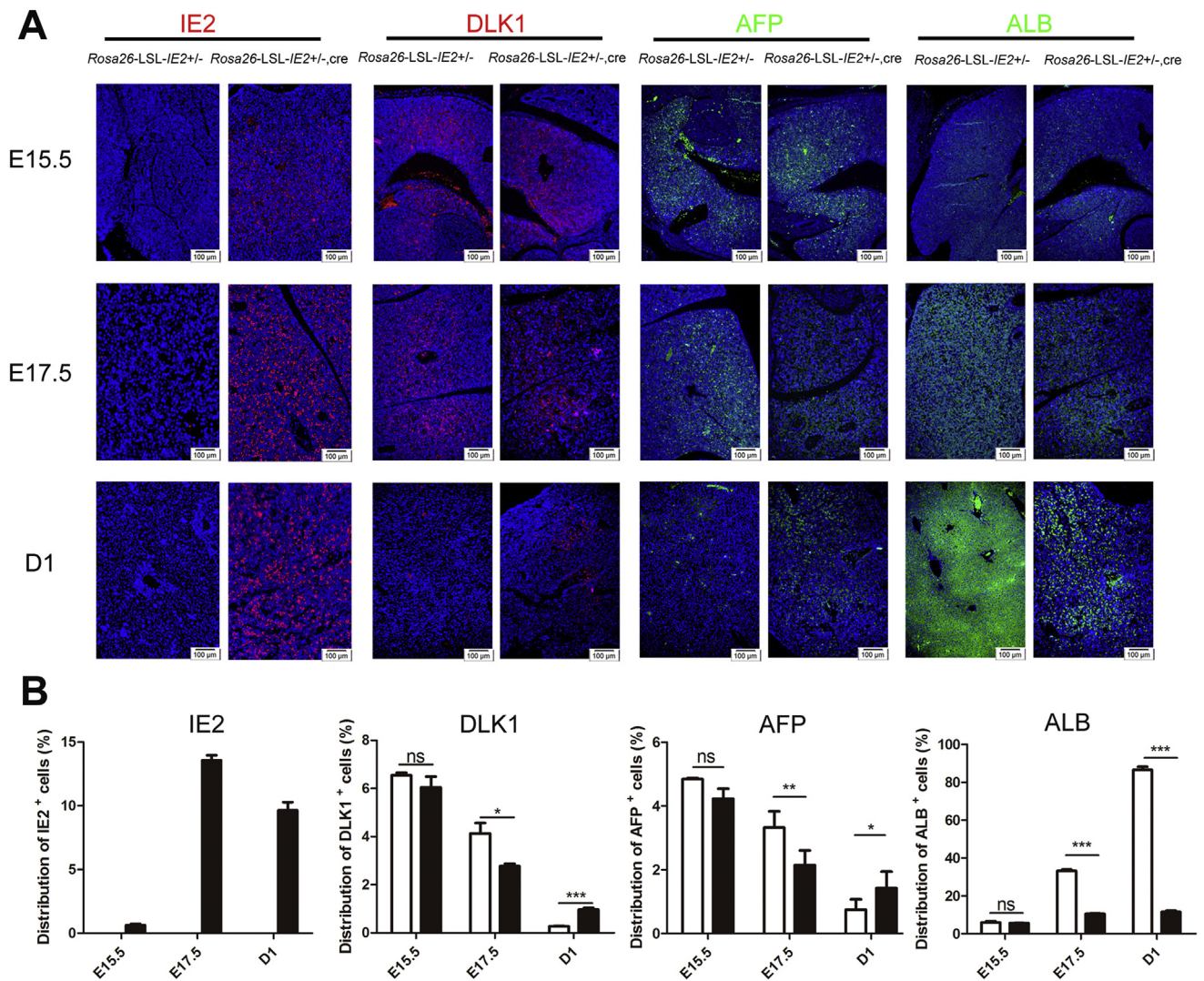


Figure 2. Effects of IE2 expression on hepatoblasts and hepatocytes during liver development. (A) Immunofluorescence at stages E15.5, E17.5, and D1 livers, with primary antibodies against IE2 (red), DLK1 (red), AFP (green), ALB (green), and Alexa Fluor 488- and 555-conjugated secondary antibodies. Scale bars: 100 μm. (B) Quantification of IE2-, DLK1-, AFP-, and ALB-positive cells from panel A. n = 3–5 mice per group. Error bars represent SEM. *P < .05, **P < .01, and ***P < .001. n = 3–5 mice per group. NS, no statistical difference.

evaluated using PPI (Figure 5A). The network showed that cyclin dependent kinase interacting protein/kinase inhibitory protein (CIP/Kip) family members, such as cyclin-dependent kinase inhibitor 1a (cdkn1a, also known as P21)

and cyclin-dependent kinase inhibitor 1b (cdkn1b, also known as P27),^{16,17} have a high degree of connectivity. In addition, the cell cycle of D1 mice also was tested by flow cytometry. It was found that the number of S-phase cells was

Table 2. Quality Control of the RNA-Sequencing Analysis

Group	Sample	Total reads	Total mapped	CleanGC	CleanQ20	CleanQ30
Rosa26-LSL-IE2 ^{+/-,cre}	B	26,578,833	92.51%	49.51; 49.38	97.57; 95.40	93.61; 90.77
	C	28,219,745	93.02%	48.81; 48.78	97.55; 95.53	93.46; 90.30
	E	23,773,646	93.17%	49.92; 49.60	97.71; 95.19	94.00; 90.52
Rosa26-LSL-IE2 ^{+/-}	IE2	25,531,997	95.93%	50.49; 50.31	97.64; 96.87	93.85; 92.57
	IE3	23,681,012	96.71%	50.42; 50.18	97.74; 97.13	94.03; 93.07
	IE4	21,074,033	96.35%	50.20; 50.04	97.56; 96.50	93.64; 91.82
Wild-type	WT1	25,010,863	93.38%	50.27; 50.19	97.41; 93.92	93.02; 87.89
	WT2	25,536,067	94.87%	50.01; 49.75	97.82; 95.43	94.17; 90.64
	WT3	31,992,416	95.30%	50.38; 50.33	97.67; 95.52	93.76; 90.42

GC, Guanine and cytosine; Q20, Quality_20; Q30, Quality_30; WT, Wild-Type.

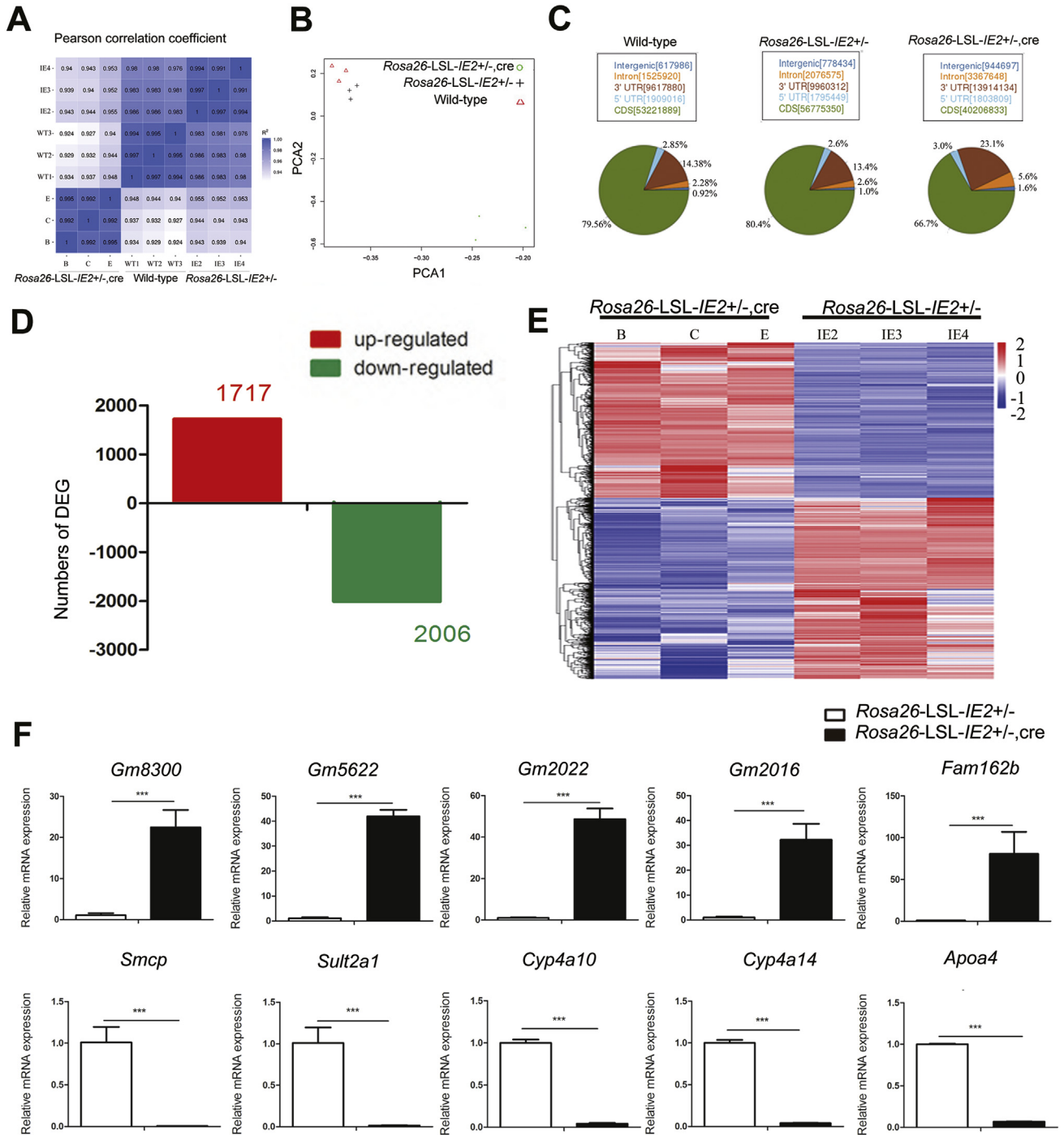


Figure 3. IE2-specific expression altered the expression level of genes in the liver. (A) Heatmap representing the correlation coefficient of samples between *Rosa26-LSL-IE2^{+/-}* mice, wild-type mice, and *Rosa26-LSL-IE2^{+/-}, cre* mice. The closer the correlation coefficient (R2) is to 1, the higher the similarity of expression patterns between samples. (B) Principal component analysis (PCA) was used to evaluate the differences between 3 groups and the repeatability of samples within groups. (C) Comparing the distribution of exon, intron, and intergenic regions of the genome to detect the source of sequence in the genome. (D) The gene number of up-regulation and down-regulation in the *Rosa26-LSL-IE2^{+/-}, cre* group compared with the *Rosa26-LSL-IE2^{+/-}* group. (E) Heatmap representing alteration of hepatic gene expression. Blue represents a down-regulation in expression and red represents up-regulation when compared with *Rosa26-LSL-IE2^{+/-}*. (F) Validation of top DEGs by quantitative real-time PCR. Top DEGs were up-regulated (up) and down-regulated (down). Error bars represent SEM. The Student *t* test was used to analyze statistical differences. ****P* < .001. n = 3 mice per group.

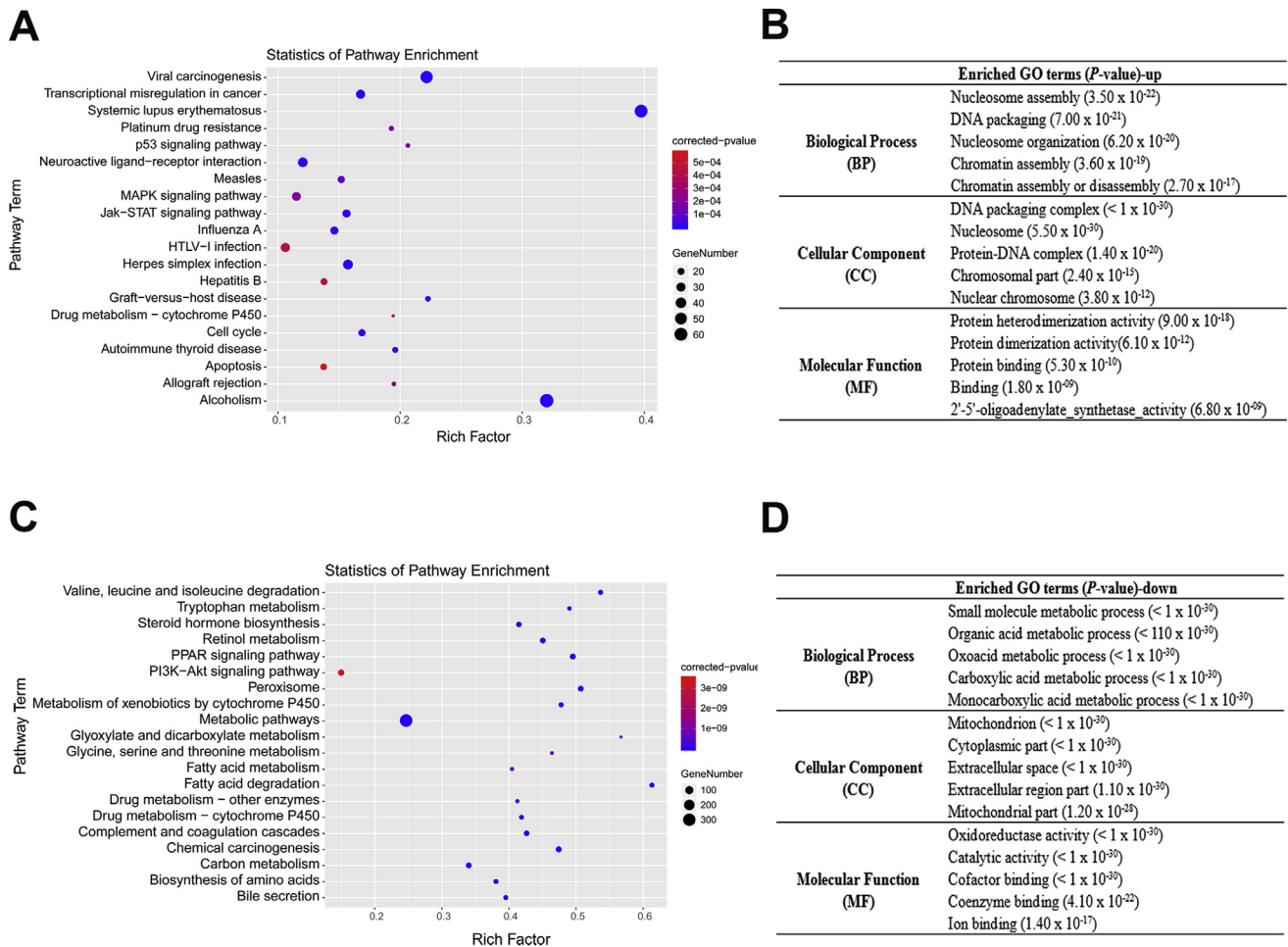


Figure 4. Main KEGG pathways and GO terms enriched by DEGs between the *Rosa26-LSL-IE2*^{+/-} and the *Rosa26-LSL-IE2*^{-/-}, cre group. (A) Top 20 up-regulation KEGG pathways. (B) Top 5 up-regulation GO terms, including BP, CC, and MF. (C) Top 20 down-regulation KEGG pathways. (D) Top 5 down-regulation GO terms, including BP, CC, and MF. BP, biological process, CC, cellular component, HTLV-1, human T-lymphotropic virus type 1; Jak-STAT, janus kinase-signal transducer and activator of transcription; MAPK, mitogen-activated protein kinase; MF, molecular function; PI3K-Akt, phosphatidylinositol 3 kinase (PI3K)/protein kinase B (AKT); PPAR, peroxisome proliferator-activated receptor.

increased in *Rosa26-LSL-IE2*^{+/-}, cre mice compared with that in *Rosa26-LSL-IE2*^{+/-} mice (Figure 5B and C). Ki67 is a nuclear antigen expressed during the proliferative phase, except in cells in the G0 phase. The proportion of Ki67-positive cells was increased significantly in *Rosa26-LSL-IE2*^{+/-}, cre mice compared with that in *Rosa26-LSL-IE2*^{+/-} mice (Figure 5D). These results suggest that numerous cells have a stagnant cell cycle that does not function properly.

However, the molecular mechanisms leading to S-phase arrest remain unknown. To understand the molecular basis underlying this, the messenger RNA (mRNA) expression and protein levels of P21 and P27 were evaluated. It was found that P21 and P27 were highly expressed in *Rosa26-LSL-IE2*^{+/-}, cre mice (Figure 5E and F). The arrest in cell-cycle progression possibly was owing to P21 and P27 inhibition. Furthermore, gamma histone variant H2AX (γ H2AX), as a marker of DNA damage and repair,¹⁸ was used to measure DNA damage, which evidently was increased in *Rosa26-LSL-IE2*^{+/-}, cre mice (Figure 5G). These data indicate that IE2

may block cell proliferation and induce DNA damage, thereby inhibiting the normal development of the liver.

Dysregulated Apoptosis in IE2-Expressing Livers

An increase in apoptosis may be a key factor in hepatic hypoplasia. To determine whether IE2 expression is involved in regulating this programmed death, flow cytometry was performed on the hepatocytes of *Rosa26-LSL-IE2*^{+/-} and *Rosa26-LSL-IE2*^{+/-}, cre mice. The proportion of apoptotic cells was increased significantly in *Rosa26-LSL-IE2*^{+/-}, cre mice, which was consistent with the KEGG enrichment analysis (Figure 6A and B). The expression levels of the death receptor *TRAIL-R* (*Tnfrsf10b*), the pro-apoptotic gene *PMAIP1*, and the apoptotic gene *caspase3* were up-regulated in *Rosa26-LSL-IE2*^{+/-}, cre mice (Figure 6C).

Next, the protein level of caspase 3 in the liver was estimated. As shown in Figure 6D, there was no caspase 3 expressed at E15.5. However, its expression was increased significantly in *Rosa26-LSL-IE2*^{+/-}, cre livers at D1, indicating

Table 3. Top 30 Genes Ranked by Degree in PPI Network

Rank	Gene name	Degree
1	<i>Ccnb1</i>	63
2	<i>Ccna2</i>	53
3	<i>Rad21</i>	45
4	<i>Jun</i>	43
4	<i>Mad2l1</i>	43
6	<i>Pcna</i>	42
6	<i>Birc5</i>	42
8	<i>Bub1</i>	41
8	<i>Cdca8</i>	41
10	<i>Stat1</i>	38
11	<i>Il6</i>	37
12	<i>Ndc80</i>	35
12	<i>Cdca5</i>	35
14	<i>Ncapg</i>	34
14	<i>Pbk</i>	34
16	<i>Sgol1</i>	31
16	<i>Irf7</i>	31
16	<i>Pomc</i>	31
19	<i>Prc1</i>	30
19	<i>Hist1h2ak</i>	30
19	<i>Hist2h2aa2</i>	30
19	<i>Hist2h2ac</i>	30
19	<i>Hist1h2ah</i>	30
24	<i>Hist1h2bb</i>	29
24	<i>Sgol2a</i>	29
24	<i>Hist1h2af</i>	29
24	<i>Cenpn</i>	29
28	<i>Rec8</i>	28
28	<i>Hist3h2ba</i>	28
28	<i>Il10</i>	28

that cell death was serious at this stage. Furthermore, it was expressed mainly in IE2-positive cells, suggesting that it may be an IE2 target responsible for the decrease in the number of hepatoblasts and hepatocytes of *Rosa26-LSL-IE2^{+/-}*, cre mice.

Hepatic Inflammation Exists in IE2-Expressing Livers

Transcriptome analysis results showed that antigen processing and presentation, cytokine-cytokine receptor interaction, and the tumor necrosis factor (TNF) signaling pathway were up-regulated in *Rosa26-LSL-IE2^{+/-}*, cre mice (Supplementary Table 2). Therefore, the expression of related genes was investigated (Figure 7A). Inflammatory cytokines *IL1 β* , *IL6*, and *TNF α* were significantly higher in *Rosa26-LSL-IE2^{+/-}*, cre mice than in *Rosa26-LSL-IE2^{+/-}* mice (Figure 7B). *Rosa26-LSL-IE2^{+/-}*, cre livers showed a scattered inflammatory cell infiltration by histology (Figure 7C). Furthermore, IE2-expressing mice showed that a distinct increase in the percentage of CD4⁺ and CD8⁺ T cells in hepatic CD3⁺ T cells, compared with those in *Rosa26-LSL-IE2^{+/-}* mice (Figure 7D and E). Immunofluorescence analysis showed IE2-expressing

liver with more CD3⁺ CD4⁺ and CD3⁺ CD8⁺ T cell infiltration (Figure 7F). These data suggest that IE2 expression may induce a certain cellular inflammatory immune reaction, but it is subject to evaluation in further studies.

Impaired Hepatocyte Maturation in IE2-Expressing Livers

Glycogen synthesis is a biochemical function of mature hepatocytes.¹⁹ Periodic acid-Schiff staining showed a marked decrease in glycogen synthesis at 17.5 days, and it was almost none at D1 in *Rosa26-LSL-IE2^{+/-}*, cre mice compared with that in *Rosa26-LSL-IE2^{+/-}* mice. However, glycogen synthesis increased continuously with liver development in *Rosa26-LSL-IE2^{+/-}* mice (Figure 8A). Next, the expression level of zonula occludens-1, which is an indicator of tight junctions, was determined to assess hepatocyte maturity (Figure 8B). Several tight junctions evidently were increased in *Rosa26-LSL-IE2^{+/-}* livers, whereas those in *Rosa26-LSL-IE2^{+/-}*, cre livers showed a dramatic decrease in number. In addition, the whole liver's metabolism at stage D1 was evaluated by gene set enrichment analysis (GSEA), and the data showed that hepatocyte maturation and metabolic function remained low overall (Figure 8C).

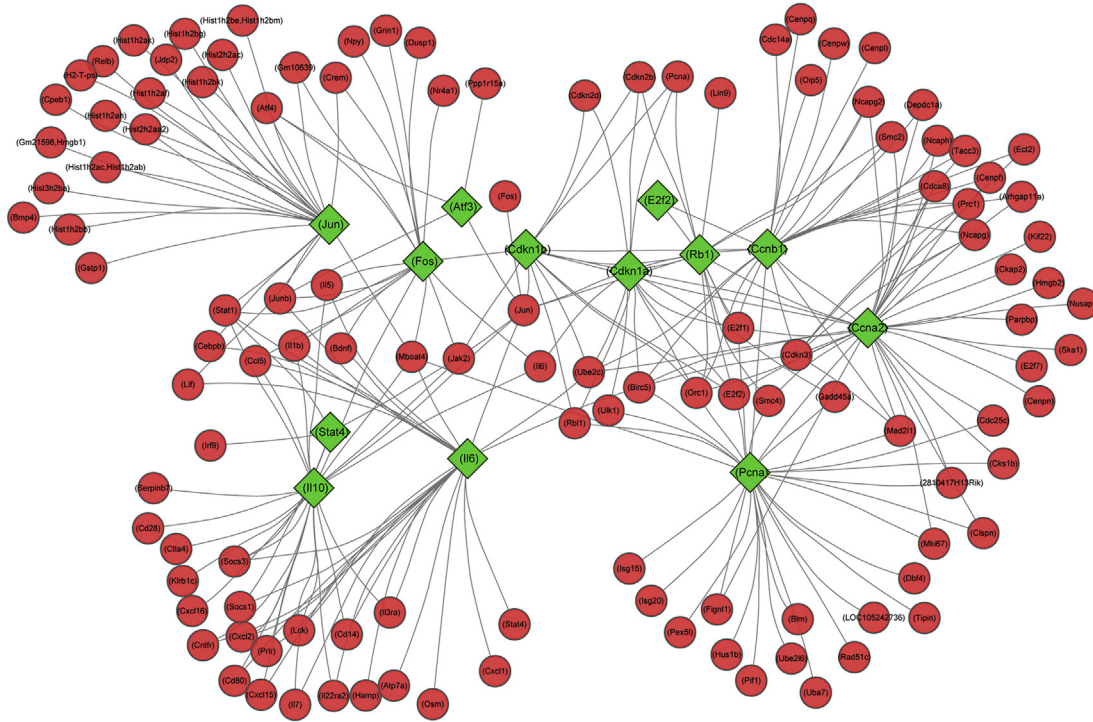
DEGs related to hepatic differentiation and maturation are shown in Figure 8D. CCAAT/enhancer binding protein alpha (C/EBP α) and hepatic nuclear factor 4 α (HNF4 α), which are key regulators of hepatocyte differentiation and maturation, controlled the expression of multiple liver-specific transcriptional genes. The mRNA and protein expression levels of C/EBP α and HNF4 α were decreased dramatically in *Rosa26-LSL-IE2^{+/-}*, cre livers at stage D1 (Figure 8E and F). Moreover, several transcriptional genes regulated by C/EBP α and HNF4 α were observed to be decreased significantly in *Rosa26-LSL-IE2^{+/-}*, cre livers at stage D1, including apolipoprotein M, A-I, A-II, C-II, and C-IV and coagulation factors XI, XII, and XIII²⁰⁻²² (Table 4). Thus, the significant decrease in C/EBP α and HNF4 α in hepatocytes appears to be a major mechanism of hepatocytes' inadequate maturation.

Discussion

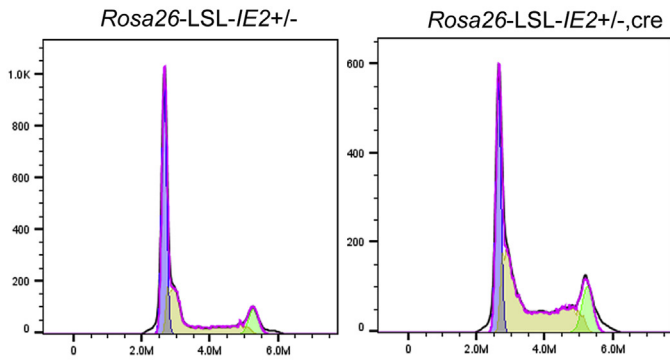
IE2 (also named IE86 and UL122), is essential for HCMV replication. Previous studies have confirmed that HCMV-induced neurodevelopmental disorders can be explained by IE2 action alone.¹⁴ Although our previous research suggested that IE2 can promote hepatic steatosis in adult mice, its effect on embryonic liver development remains rarely reported. In this study, transgenic mice (*Rosa26-LSL-IE2^{+/-}*, cre) were constructed to simulate the pathology of the effect of IE2 expression on cells after HCMV infection and explore the effect of IE2 on the embryonic liver. It was found that long-term IE2 expression disrupts the liver's normal development by impairing the program of hepatocyte proliferation, apoptosis, and maturation, which may be responsible for the lethality at E17.5-D1.

The death of *Rosa26-LSL-IE2^{+/-}*, cre mice at late embryonic stage was unexpected. Our research team also constructed an animal model that specifically expressed

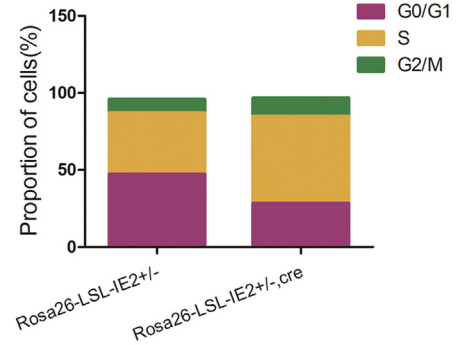
A



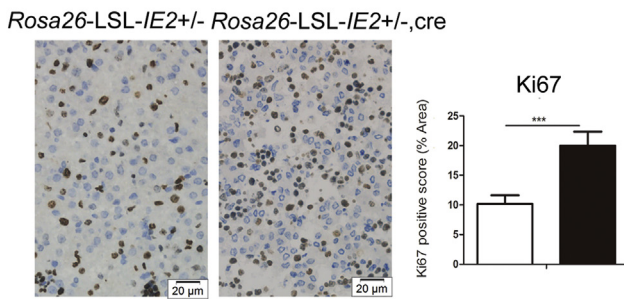
B



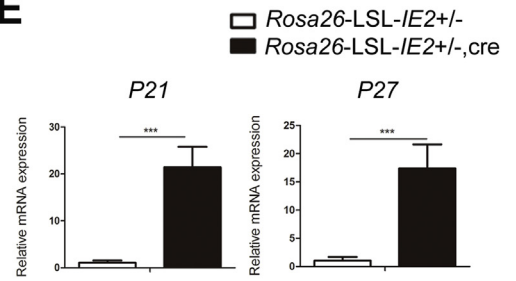
C



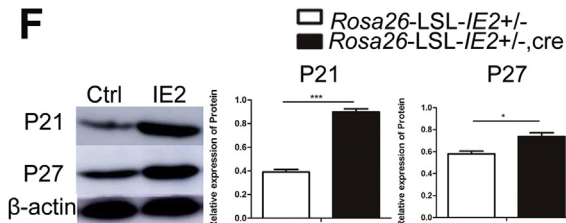
D



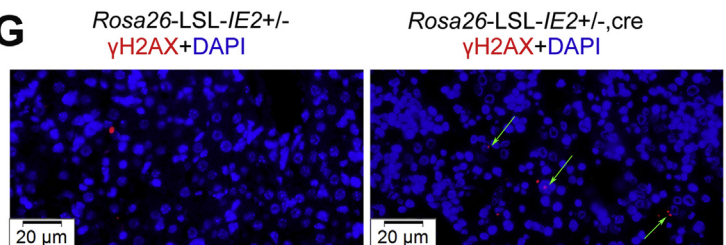
E



F



G



IE2 in the hippocampus; it showed that IE2 expression only causes hippocampus damage in mice, but it does not affect their survival.²³ The development of fetal liver plays a key role in the whole life cycle. Based on these findings, we proposed here that late embryonic lethality could be owing to hepatic hypoplasia caused by long-term and stable IE2 expression in the liver. However, the precise causes leading to this occurrence must be investigated and debated further.

During embryogenesis, the timing of the hepatoblast-to-hepatocyte transition occurs between E13.5 and E15.5, after which hepatocytes increase until adulthood.²⁴ In contrast, IE2-expressing mice showed a tremendously slower increase in the number of hepatocytes from E17.5 to D1 compared with that in the control group of this study. The hypoplasia observed in the livers of *Rosa26-LSL-IE2^{+/-}*, cre mice was associated with the inhibition of hepatocellular proliferation. Most cells were halted in S-phase in *Rosa26-LSL-IE2^{+/-}*, cre mice. Murphy et al²⁵ also confirmed that IE2 protein could induce more cells to enter the S-phase and to halt the cell cycle. Han et al¹⁴ showed that IE2 expression, but not IE1, induces host cell-cycle arrest by cell-cycle-inhibitory and DNA binding activities, leading to the impairment of brain development. We also identified 2 potential target genes that might account for the growth arrest in hepatocytes: *P21* and *P27*. A previous study showed that *P21*, overexpressing in hepatocytes, which dramatically inhibited hepatocyte proliferation, resulting in aberrant tissue organization, impeded liver and body growth, and increased mortality.²⁶ These data might suggest that the expression of IE2 hindered cell-cycle processes, which may be an important factor for developmental liver arrest.

On the other hand, we also observed that apoptosis of hepatocytes significantly increased in *Rosa26-LSL-IE2^{+/-}*, cre mice. Studies have confirmed that cell apoptosis is one mechanism by which hypocellularity can occur in the developing liver. Previous studies have reported that HCMV disrupts apoptosis through the external (extracellular ligands and death receptors) and internal apoptosis pathways (endoplasmic reticulum stress, lysosomal dysfunction, and mitochondrial dysfunction).²⁷ Chien and Dix²⁸ detected significant amounts of TNF- α , TNF receptors 1 and 2, active caspase 8, active caspase 3, *TRAIL*, *TRAIL-R*, *FAS*, and *FASL* mRNAs and/or proteins in murine cytomegalovirus-infected eyes. Chiou et al²⁹ reported that IE2, but not IE1, up-regulates *FASL* expression and promotes HCMV-infected human retinal pigment epithelium cell apoptosis. In our study, *Tnfrsf10b*, *Pamip1*, and *Caspase 3* were highly expressed in IE2-

expressing mice. In addition, immunofluorescence results showed that the expression of caspase 3 was higher in D1 than in E17.5 mice, which was contrary to the trend of ALB expression during liver development. In addition, IE2-expressing liver showed higher expression of inflammatory factors, which may promote cell apoptosis. Hence, the continuing accumulation of IE2 damaged hepatocyte survival and resulted in serious hepatic hypoplasia.

In addition to the dramatic decrease of hepatocytes in IE2-expressing livers, we also found inadequate maturation of hepatocytes, characterized by diminished glycogen storage, decrease of drug metabolic activity (Figure 4C), and significantly lower expression of factors associated with hepatocyte function such as apolipoproteins, transthyretin, aldehyde dehydrogenase, and coagulation factors. Cell metabolomic studies have evaluated the primary infection of HCMV involved in the dysfunction of cellular metabolism, leading to a variety of amino acid, fatty acid, and energy metabolism disorders.^{7,30,31} Furthermore, in our study, we also observed a lower expression in the regulators of hepatocyte maturation, such as *C/EBP α* and *HNF4 α* . *C/EBP α* is a critical regulator of hepatocyte metabolic function by transcriptional control of multiple downstream factors, such as apolipoprotein M and A-I, several coagulation factors, and transthyretin.³² *HNF4 α* is essential for morphologic and functional differentiation of hepatocytes, accumulation of hepatic glycogen stores, and generation of a hepatic epithelium.³³ Further research is necessary to verify whether IE2 directly controls the expression of *C/EBP α* and *HNF4 α* . Overall, impaired hepatocyte maturity was inadequate to sustain hepatic or fetal viability.

This study had several limitations. First, given that HCMV has a large and complicated genome, our results could not sufficiently explain the mechanism of liver diseases with congenital HCMV infection. Second, the expression level of IE2 after HCMV infection in human beings is unknown because of a lack of research. Thus, the results of this study only speculate the effect of IE2 on liver after HCMV infection. Further studies and clinical data are needed to support the specific situation of fetal liver with HCMV infection.

In summary, the *Rosa26-LSL-IE2^{+/-}*, cre mice that stably expressed IE2 in the liver were constructed successfully. Based on this transgenesis mouse model, our results showed that IE2 may play a key role in HCMV-caused liver disorders. The long-term expression of IE2 inhibited hepatocyte proliferation, increased cell apoptosis, and impaired their maturation, resulting in liver hypoplasia. Moreover, our findings provide valuable resources to further elucidate

Figure 5. (See previous page). Effects of IE2 expression on cell cycle and DNA damage. (A) Network of PPI of cell cycle-related DEGs between *Rosa26-LSL-IE2^{+/-}* and *Rosa26-LSL-IE2^{+/-}*, cre mice. Green represents a regulatory gene, red represents a target gene. (B) The cell cycles were detected by flow cytometry between D1 *Rosa26-LSL-IE2^{+/-}* and *Rosa26-LSL-IE2^{+/-}*, cre mice. (C) Proportional distribution of cells in G0, S, and G2/M stages of the cell cycle. (D) D1 liver sections stained with immunostained for Ki67 (left). Quantification of Ki67-positive cells (right). (E) mRNA expression levels of *P21* and *P27* were measured by quantitative real-time PCR. (F) The protein expression levels of *P21* and *P27* were measured by Western blot (left). Quantification of *P21* and *P27* expression (right). (G) Comparison of DNA damage between D1 *Rosa26-LSL-IE2^{+/-}* and *Rosa26-LSL-IE2^{+/-}*, cre mice. γ H2AX is a marker of DNA damage. Green arrows represent DNA damage. Scale bars: 20 μ m. Ctrl represents *Rosa26-LSL-IE2^{+/-}*, IE2 represents *Rosa26-LSL-IE2^{+/-}*, cre. Error bars represent SEM. The Student *t* test was used to analyze statistical differences. **P* < .05, ****P* < .001. *n* = 3 mice per group. Ctrl, control; DAPI, 4', 6-diamidino-2-phenylindole.

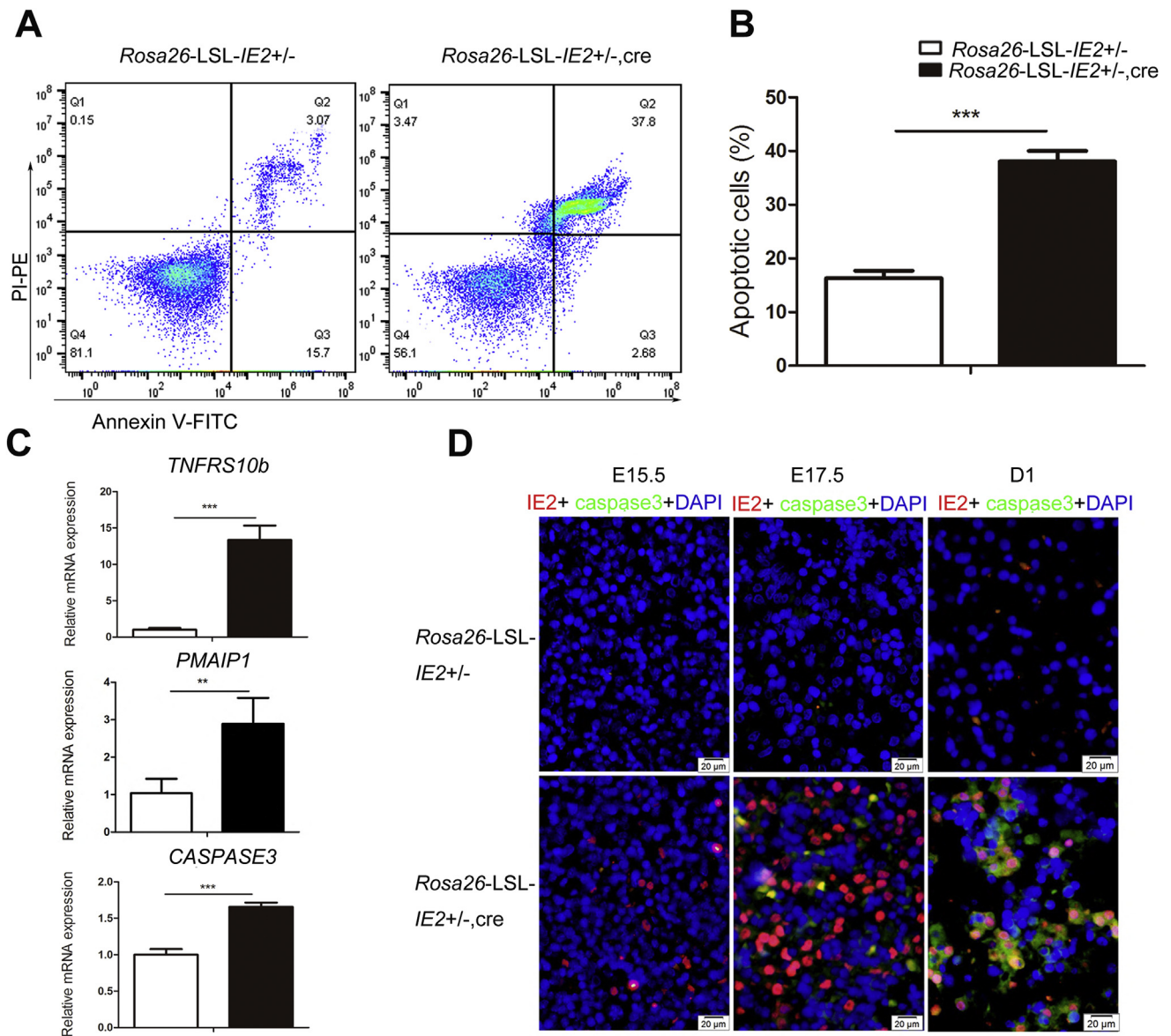


Figure 6. IE2-specific expression promotes cell apoptosis. (A) The cell apoptosis was detected by flow cytometry between D1 *Rosa26-LSL-IE2^{+/-}* and *Rosa26-LSL-IE2^{+/-}, cre* mice. (B) Proportional distribution of fluorescein isothiocyanate (FITC)+ PI+ cells. (C) mRNA expression levels of the apoptosis-related genes were measured by quantitative real-time PCR. (D) Immunofluorescence for E15.5, E17.5, and D1 livers, with primary antibodies against IE2 (red), caspase 3 (green), and Alexa Fluor 488- and 555-conjugated secondary antibodies. Error bars represent SEM. The Student *t* test was used to analyze statistical differences. ***P* < .01, ****P* < .001. *n* = 3–5 mice per group. DAPI, 4', 6-diamidino-2-phenylindole.

the potential cellular and molecular mechanisms of HCMV infection and to develop novel strategies to overcome related pathologies during liver development.

Materials and Methods

Animals

CRISPR/cas9 technology was used to construct *Rosa26-LSL-IE2^{+/-}* mice. *Rosa26-LSL-IE2^{+/-}* and albumin-Cre mice were used to obtain *Rosa26-LSL-IE2^{+/-}, cre* mice (Figure 9). All mice were housed and maintained under specific pathogen-free conditions on a 12-hour day/night cycle at 23°C ± 2°C and received an autoclaved standard diet and

water ad libitum. Mice were mated overnight, and the vaginal plug was detected at the noon as E0.5. The *Rosa26-LSL-IE2^{+/-}, cre* mice were identified by PCR. The *Rosa26-LSL-IE2^{+/-}* mice were control mice. The sequences of primers are listed in Table 5. All animal experiments were performed according to the guidelines of the Animal Welfare and Research Ethics Committee of Qingdao University.

Sample Collection

Embryos were collected on E15.5, E17.5, and D1, and fixed in 4% paraformaldehyde for 24 hours. Embryos were embedded in paraffin and sectioned at 5–6 μm. Liver tissues were stored in liquid nitrogen.

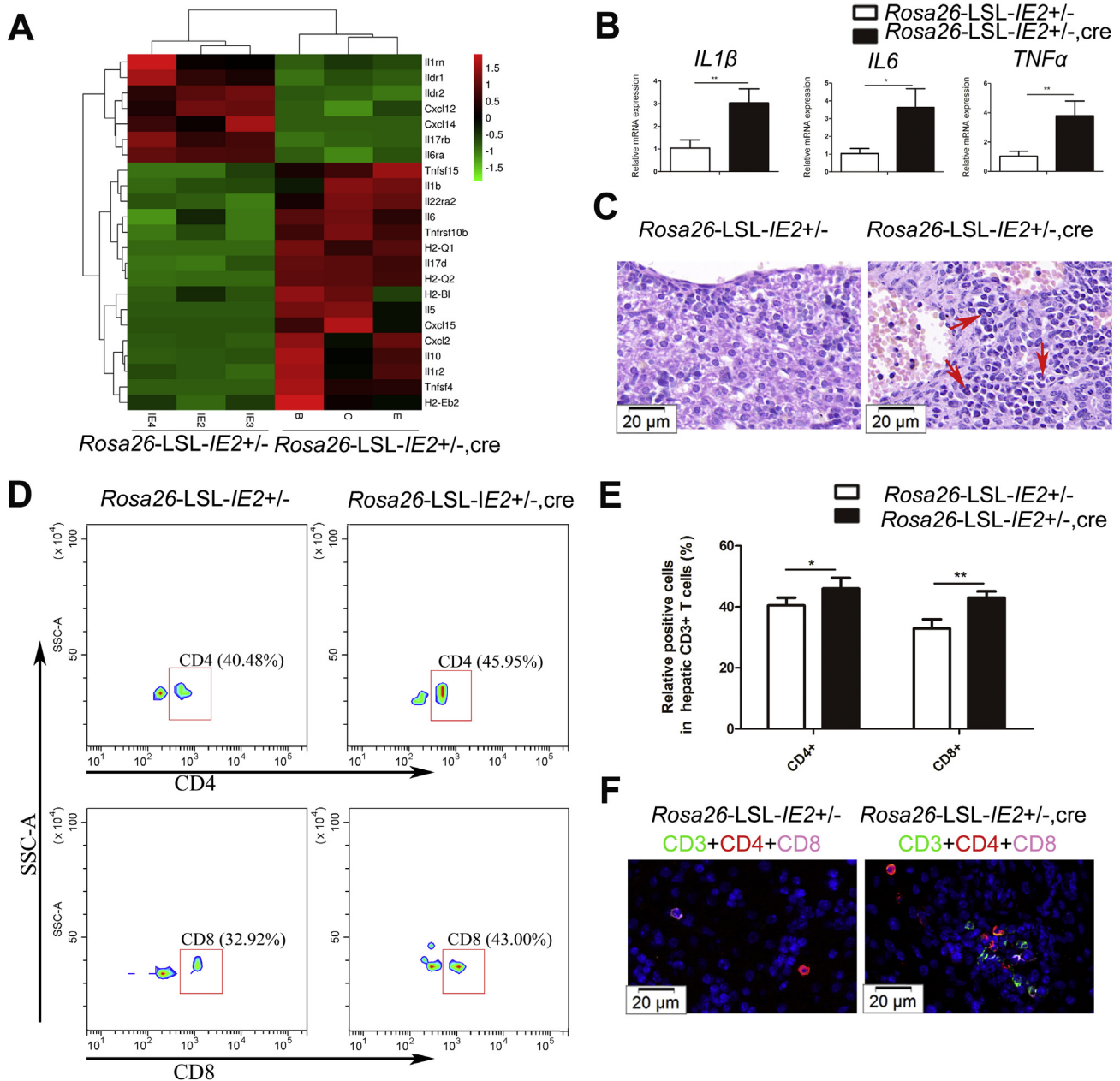


Figure 7. The inflammatory milieu in *Rosa26-LSL-IE2^{+/-}, cre* livers. (A) Heatmap representing expression of genes related to an inflammatory response. (B) mRNA expression levels of *IL1β*, *IL6*, and *TNFα* were measured by quantitative real-time PCR. (C) H&E showed scattered inflammatory cell infiltration (red arrows) in *Rosa26-LSL-IE2^{+/-}, cre* livers. Scale bars: 20 μm. (D) The percentage of CD4⁺ and CD8⁺ T cells in hepatic CD3⁺ T cells was detected by flow cytometry. The cells were analyzed by a fluorescence-activated cell sorter. (E) Summarized data of panel D. (F) Immunofluorescence for D1 livers, with primary antibodies against CD3 (green), CD4 (red), CD8 (pink), and Alexa Fluor 488- and 555-conjugated secondary antibodies. Scale bars: 20 μm. Error bars represent SEM. The Student *t* test was used to analyze statistical differences. **P* < .05, ***P* < .01. *n* = 3–5 mice per group. SSC, side scatter.

Total RNA Extraction and Transcriptomic Analysis

Total liver RNA was extracted by TRIzol reagent following the manufacturer's instructions (Invitrogen, Carlsbad, CA). The quantity and purity of RNA were analyzed using Bioanalyzer 2100 and the RNA 6000 Nano LabChip Kit (Agilent, Folsom, CA). After purification, the

poly (A) - or poly (A) + RNA fractions was fragmented into small pieces by using divalent cations under increased temperature. Then, the cleaved RNA fragments were reverse-transcribed to create the final complementary DNA library in accordance with the protocol for the mRNA-sequencing sample preparation kit (Illumina, San Diego, CA), the average insert size for the paired-end libraries was 300 bp

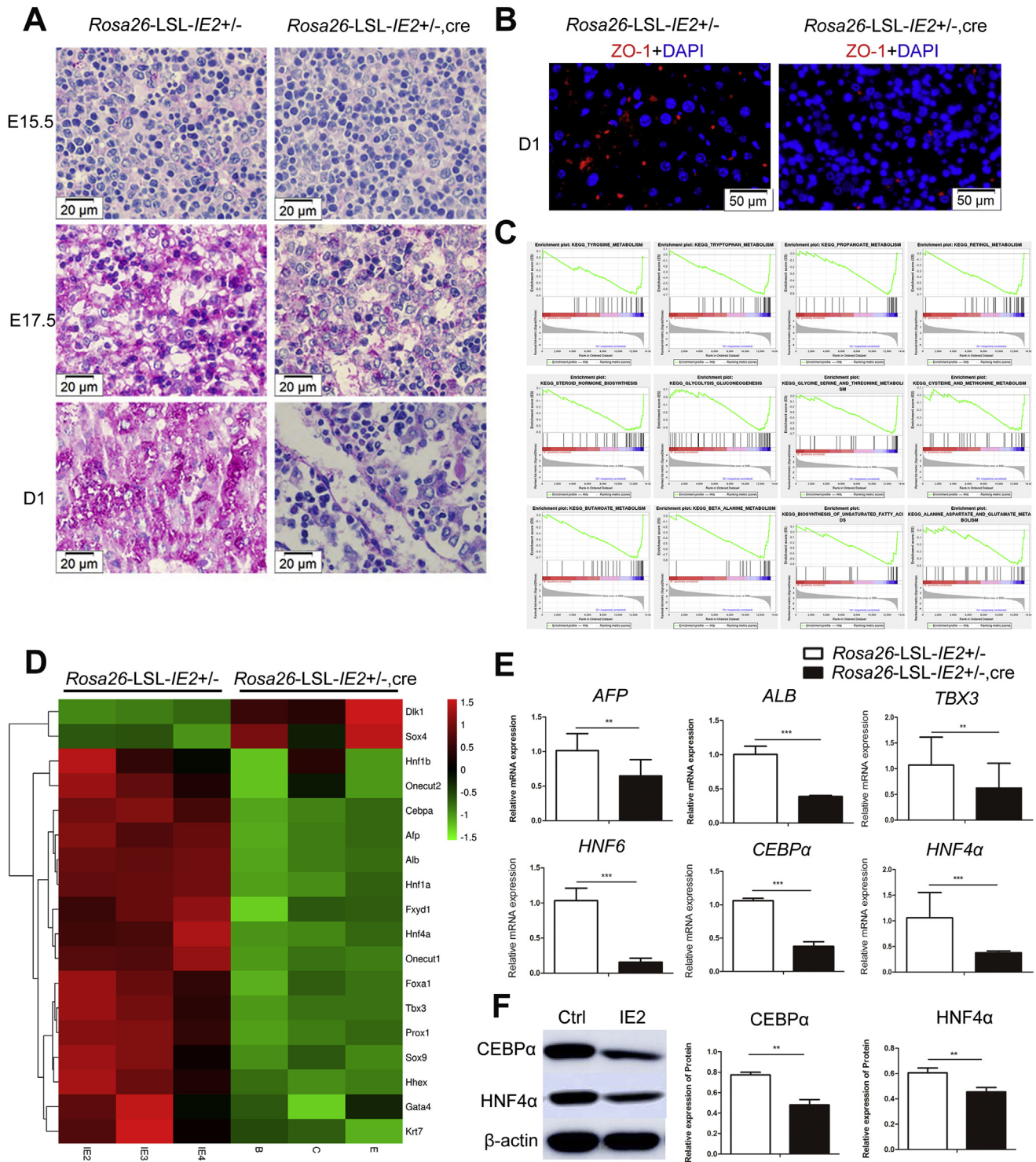


Figure 8. Inadequate maturation of remnant hepatocytes in *Rosa26-LSL-IE2^{+/-}, cre* livers. (A) Hepatocellular cytoplasmic glycogen stores stained with periodic acid–Schiff. Scale bars: 20 μ m. (B) Immunofluorescence for zonula occludens-1 (ZO-1) showed tight junctions in the D1 livers. Scale bars: 20 μ m. (C) GSEA showing target metabolism pathways. Heatmap representing alteration of gene expression enriched in hepatocyte differentiation and maturation. Green represents a down-regulation in expression and red represents up-regulation when compared with the *Rosa26-LSL-IE2^{+/-}* group. (D) mRNA expression levels of the major cell markers and important transcription factors were measured by quantitative real-time PCR. (E) The protein expression levels of CEBP α and HNF4 α were measured by Western blot (left). Quantification of CEBP α and HNF4 α expression (right). Ctrl represents *Rosa26-LSL-IE2^{+/-}*, IE2 represents *Rosa26-LSL-IE2^{+/-}, cre*. Error bars represent SEM. The Student *t* test was used to analyze statistical differences. ***P* < .01, ****P* < .001. n = 3–5 mice per group. Ctrl, control; DAPI, 4', 6-diamidino-2-phenylindole.

Table 4. Transcriptome Sequencing Analysis of D1 Livers Show Differences in Hepatocyte Maturation

Gene name	<i>Rosa26-LSL-IE2</i> ^{+/-}	<i>Rosa26-LSL-IE2</i> ^{+/-} ,cre	log ₂ fold change
<i>Apom</i>	20,732.8	3823.803	-2.4
<i>Apoa1</i>	539,948	161,932.1	-1.7
<i>F11</i>	6166.915	580.1111	-3.4
<i>Cebpa</i>	8919.249	2988.301	-1.6
<i>Ttr</i>	92,307.05	21,216.03	-2.1
<i>Aldh8a1</i>	7154.736	483.6135	-3.9
<i>Hp</i>	151,217.9	15,128.83	-3.3
<i>F7</i>	1882.091	436.3027	-2.1
<i>F10</i>	23,025.82	5290.734	-2.1
<i>F13b</i>	10,956.96	2364.134	-2.2
<i>F5</i>	10,192.95	3992.128	-1.4
<i>Trf</i>	1,344,075	313,306.7	-2.1
<i>Pzp</i>	181,941.8	20,681.85	-3.1
<i>Hnf4a</i>	18,749.25	3782.18	-2.3
<i>Apob</i>	105,442.6	43,189.55	-1.3
<i>Apoa2</i>	70,310.33	5747.637	-3.6
<i>Apoc4</i>	8514.516	779.1263	-3.5
<i>Apoc2</i>	540.3241	38.43124	-3.8

(±50 bp).³⁴ Then, the paired-end sequencing on an Illumina Novaseq was performed at the Berry Genomics Corporation (Beijing, China) following the vendor's recommended protocol.

Bioinformatics Analysis

First, the spliced, repetitive, low-sequencing-quality reads were filtered out by Cutadapt (<https://cutadapt.readthedocs.io/en/stable/installation.htm>). Then, the sequence quality was verified by FastQC (<http://www.bioinformatics.babraham.ac.uk/projects/fastqc>). The reads were mapped to the reference genome of mouse (mm10) by hisat2 software (<http://daehwankimlab.github.io/hisat2/>) for similarity analysis.³⁵ Quantitative analysis of the gene expression level was performed by feature count software and the DEGs were analyzed by edgeR software. The fold change of mRNA greater than 1.5 and $P < .05$ were considered to be the DEGs. GO and KEGG pathways were analyzed by topGO (https://rpubs.com/aemoore62/TopGo_colMap_Func_Troubleshoot) and KOBAS software (<http://kobas.cbi.pku.edu.cn/download.do>). GSEA was performed by GSEA 3.0 software (<http://software.broadinstitute.org/gsea/index.jsp>) to determine whether a predefined set of genes was significantly different between the 2 groups. The PPI network was created by STRING 11.0 (<https://string-db.org>), and cytoscape 3.2 (<https://cytoscape.org/download.html>) was used to screen the most important gene (hub gene) among these DEGs. The hub genes were ranked by the degree in PPI network.

Quantitative Real-Time PCR

RNA was extracted by the RNEasy kit (TIANGEN, Beijing, China), and complementary DNA was synthesized by using the Superscript kit (Roche, Basel, Switzerland). The

interested genes were quantified using quantitative real-time PCR, and performed on a Roche 480 Real Time System. The primers were synthesized by Sangon Biotech (Shanghai, China). The primer sequences are listed in Table 6. The $2^{-\Delta\Delta CT}$ method was used to determine the relative expression of the target genes normalized to *GAPDH*.

H&E staining

Approximately 3- μ m paraffin-embedded tissue sections were stained with H&E and examined by a light microscope (Olympus, Tokyo, Japan).

Immunofluorescence

Paraffin-embedded sections were deparaffinized, rehydrated, and placed in water for 5 minutes, and then antigen retrieval was performed using a sodium citrate buffer (pH 6.0) for 10 minutes in a microwave oven. After, the sections were blocked in 5% bovine serum albumin and 0.05% Triton X-100 (Solarbio, Beijing, China) for 30 minutes before application of primary antibody overnight at 4°C. The following day, sections were washed and incubated with a secondary antibody at 1:500 for 60 minutes. Sections were washed, incubated with 4', 6-diamidino-2-phenylindole containing a fluorescent inhibitor for 5 minute, and then sealed by coverslip. Primary antibodies were as follows: DLK1 (1:200, cat. BF0433; Affinity, Colorado, USA), AFP (1:100, cat. A17898; ABclonal, Wuhan, China), ALB (1:50, cat. 66051-1-Ig; Proteintech, Chicago, IL), CD3 (5 ug/mL, cat. NB600-1441; NOVUS, Centennial, CO), CD4 (1:200, cat. NBP1-19371; NOVUS, Centennial, CO), CD8 (1:100, cat. NB200-578; NOVUS, Centennial, CO), zonula occludens-1 (1:100, cat. A0659; ABclonal, Wuhan, China), caspase 3

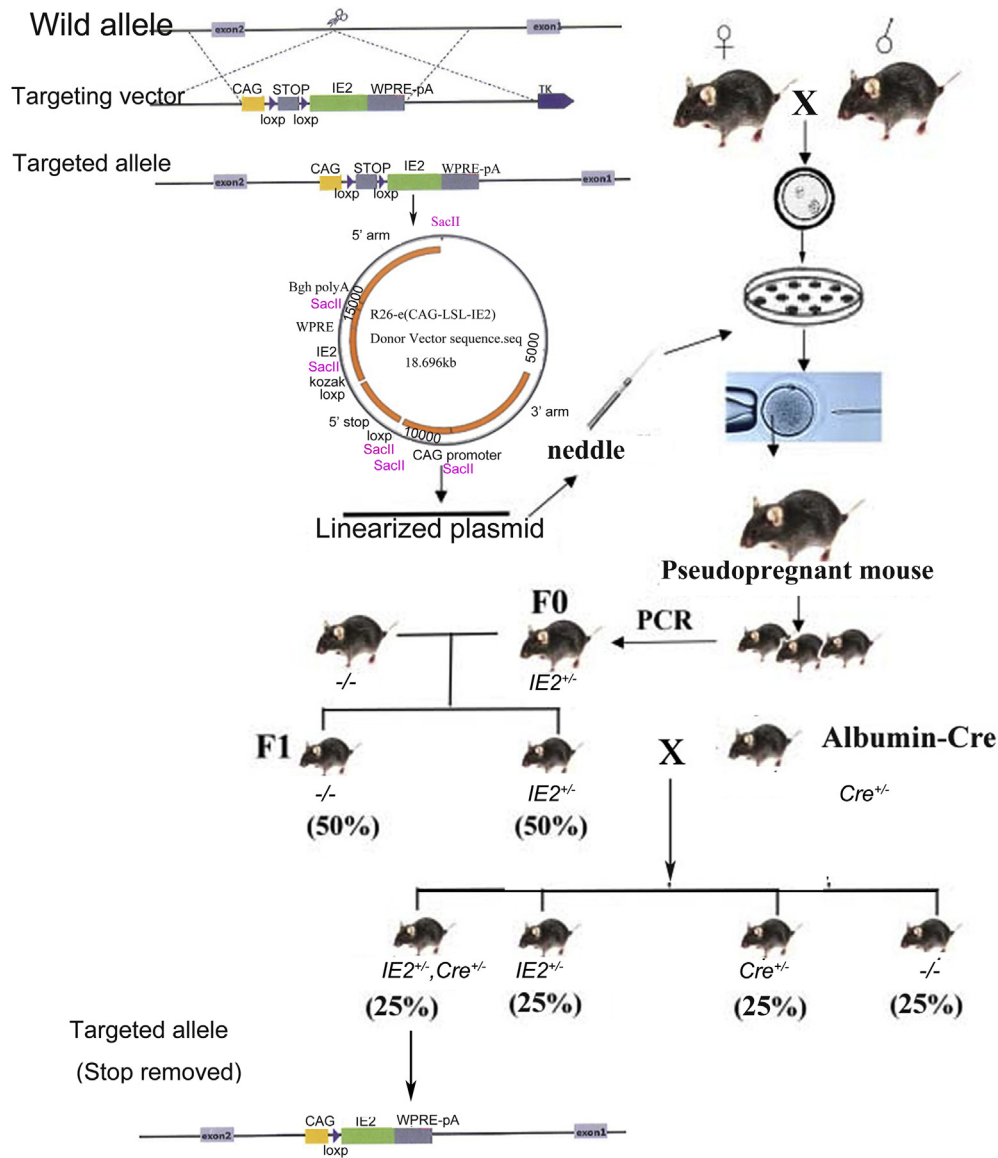


Figure 9. Construction of *Rosa26-LSL-IE2^{+/-}*, *cre* mice. First, *Rosa26-LSL-IE2^{+/-}* model mice were constructed. Next, *Rosa26-LSL-IE2^{+/-}*, *cre* mice were obtained by *Rosa26-LSL-IE2^{+/-}* mice mating with albumin-*Cre* mice. *IE2^{+/-}* represents *Rosa26-LSL-IE2^{+/-}*; *Cre^{+/-}* represents *Rosa26-LSL-IE2^{+/-}*, *cre*. Amp, ampicillin resistance screening gene; CAG, CAG promoter; loxp, locus of X-overP1; *Sac*II represents *Sac*II Restriction Endonuclease; STOP represents transcription termination element; WPRE, Woodchuck hepatitis virus post-transcriptional regulatory element; *-/-*, wild-type, *IE2^{+/-}*.

(1:100, cat. A11319; ABclonal, Wuhan, China), and CMV-IE1 and IE2 (1:100, cat. ab53495; Abcam, Cambridge, UK), and secondary antibodies used were goat anti-mouse-Cy3

(Bioss, Beijing, China) and goat anti-rabbit fluorescein isothiocyanate (Bioss, Beijing, China) at 1:500. Images were captured on an Olympus Fluoview FV1200 microscope as

Table 5. The Sequence of Real-Time PCR Primers of *Rosa26-LSL-IE2^{+/-}*, *cre* Mice

Primer name	Forward, 5'-3'	Reverse, 5'-3'	Product size
<i>Alb</i>	TTGGCCCTTACCATAACTG	GAAGCAGAAGCTTAGGAAGATGG	390 bp
<i>Wild type</i>	TCAGATTCTTTTATAGGGGACACA	TAAAGGCCACTCAATGCTCACTAA	994 bp
<i>IE2</i>	TCAGATTCTTTTATAGGGGACACA	ACGCTATGTGGATACGCTGCT	414 bp

Table 6. The Sequence of the Primers for Quantitative Real-Time PCR

Gene name	Forward, 5'-3'	Reverse, 5'-3'	Product size
<i>Gm8300</i>	AGAGTATGCCAGGTGACCAAAATG	CTCTTATGTGGCACAGCCTCCTTAC	89 bp
<i>Gm2022</i>	TCAGGTGACCAAAATGCTGGGATG	CTCTTATGTGGCACAGCCTCCTTAC	80 bp
<i>Gm5662</i>	TCAGGTGACCAAAATGCTGGGATG	CTCTTATGTGGCACAGCCTCCTTAC	80 bp
<i>Gm2016</i>	TCAGGTGACCAAAATGCTGGGATG	CTCTTATGTGGCACAGCCTCCTTAC	80 bp
<i>Fam162b</i>	CTGCTTTGCTGTGATTGTGTCTGC	CTTCACGCCACTTAGCTTTCTTTGC	95 bp
<i>Cyp4a10</i>	CTGCTCCTGCTGCTGGTAAAAG	GAGGTGATGGGAACTGCTGGAAAAG	85 bp
<i>Apoa4</i>	GCTGGTGCCCTTTGTCGTACAG	TCATGCGGTCACGTAGGTCCTC	104 bp
<i>Smcp</i>	GCTCAACCTACCTGCTGCTCTTC	ACTTCTTCTGGTTCCAGTTGCCTTG	133 bp
<i>Cyp4a14</i>	GCCATTCTCAGGAGATCAAGGAAC	AATTCAAAGCGGAGCAGGGTCAG	96 bp
<i>Sult2a1</i>	TGGAACCGCTCACCTGGATAG	GATCGCCTTGGCCTTGGAACTG	138 bp
<i>Cdkn1b</i>	GAAATCTCTTCGGCCCGGTCAATC	CGTGACTCGCTTCTCCATATCC	85 bp
<i>Cdkn1a</i>	TCCTGGTGATGCCGACCTGTTC	ACGAAGTCAAAGTTCCACCGTTCTC	150 bp
<i>HNF4α</i>	GTGCCAACCTCAATTCATCCAACAG	TCCTCACGCTCCTCTGAAGAAC	135 bp
<i>CEBPα</i>	TCGGTGGACAAGAACAGCAACG	CGGTCATTGTCAGTGGTCAACTCC	140 bp
<i>HNF6</i>	GCTATGCCACCGACAAGATGC	ATGAGGATGGTGGGAGGAAGG	144 bp
<i>TBX3</i>	TCCTCTGGCTCAGTGTCTTGTGTC	AGACCTGTCTGGCTTGGCTTCC	117 bp
<i>ALB</i>	GCAGATGACAGGGCGGAAGCTTG	AGACAGTGGGCTTTCTTCAACAGTG	110 bp
<i>AFP</i>	ATCACACCCGCTTCCCTCATCC	CATTCTTCTCCGTCACGCACTGG	118 bp
<i>PMAIP1</i>	CACCGGACATAACTGTGGTTCTGG	GAGCACACTCGTCCTTCAAGTCTG	111 bp
<i>TNFRSF10b</i>	GAAGACTGGAGCATGGAGGCAATG	CAGGTTCCGTGTGTGGTTAGAGTC	146 bp
<i>CASPASE3</i>	TCTGACTGGAAGCCGAAACTCTTC	GTCCCACTGTCTGTCTCAATGCC	84 bp

indicated in the figure legends and processed with ImageJ software (National Institutes of Health, Bethesda, MD).

Immunohistochemistry Staining

Liver tissues were fixed with 4% formalin and embedded in paraffin. Paraffin-embedded liver sections (5 μ m) were deparaffinized, rehydrated, and soaked in boiling water diluted with sodium citrate buffer (pH 6.0) for 6 minutes to repair the antigen.³⁶ Endogenous catalase was inactivated with 3% hydrogen peroxide. Then, sections were incubated with anti-mouse Ki67 (1:100, cat. A16919; ABclonal, Wuhan, China) and anti-mouse CMV-IE1 and IE2 (1:100, cat. ab53495; Abcam, Cambridge, UK) overnight at 4°C. The following morning, sections were incubated with the secondary antibodies in the incubator for 40 minutes. After washing with distilled water and phosphate-buffered saline, sections were exposed to 3,3'-diaminobenzidine tetra hydrochloride for 1 minute, hematoxylin for 1 minute, differentiate solution for 1 second, and observed after the neutral gum seal.

Western Blot

The liver tissues were isolated and pestled, and were lysed in radioimmunoprecipitation assay buffer. Sodium dodecyl sulfate-polyacrylamide gel electrophoresis was performed to separate equal amounts of cell lysates, and were transferred to a polyvinylidene difluoride membrane (Millipore, Burlington, MA). After incubation with the primary antibodies overnight at 4°C, and corresponding

secondary antibodies for 2 hours at room temperature. Finally, dropped electrochemiluminescence liquid for 1 minute, signals were detected using a chemiluminescence instrument (Imagequant LAS500, Cytiva, USA). Primary antibodies were as follows: CMV-IE1 and IE2 (1:500, cat. ab53495; Abcam, Cambridge, UK), P27 (1:1000, cat. A16722; ABclonal, Wuhan, China), P21 (1:1000, cat. bs-55160R; Bioss, Beijing, China), CEBP α (1:1000, cat. A0904; ABclonal, Wuhan, China), HNF4 α (1:1000, cat. A13998; ABclonal, Wuhan, China), and β -actin (1:2000; Santa Cruz, CA). The secondary antibodies used were horseradish peroxidase-conjugated sheep anti-mouse IgG (1:500; Absin, Shanghai, China) and anti-rabbit (1:10,000; Absin, Shanghai, China).

Analysis of Flow Cytometry and Cell Staining

The livers were taken to prepare single-cell suspensions. Single-cell suspensions were added to an Eppendorf tube (Eppendorf, Hamburg, Germany, 1×10^5 per tube) in 100 μ L phosphate-buffered saline. Annexin V-fluorescein isothiocyanate/Propidium Iodide (Biolegend) was used to detect cell apoptosis.³⁷ PI dye (Abcam) was applied to the cell cycle.³⁸ Specific antibodies were used for staining on the cell surface. The antibodies used were as follows: anti-CD3-Pacific Blue (cat. 100214; Biolegend), anti-CD4-Brilliant Violet 605 (cat. 100451; Biolegend), and anti-CD8-Allophycocyanin (cat. 100714; Biolegend); all antibodies were anti-mouse antibodies. Finally, the cells were analyzed using a fluorescence-activated cell sorter,

and the data were analyzed using FlowJo-V10 (<https://www.flowjo.com/solutions/flowjo>).

Statistical Analysis

All statistical analyses were performed using GraphPad Prism V4.0 (GraphPad Software, Inc, La Jolla, CA). Data are represented as means \pm SEM and were analyzed by a 2-tailed Wilcoxon rank-sum test. $P < .05$ was accepted as statistically significant.

All authors had access to the study data and reviewed and approved the final manuscript.

References

1. Leruez-Ville M, Foulon I, Pass R, Ville Y. Cytomegalovirus infection during pregnancy: state of the science. *Am J Obstet Gynecol* 2020;223:330–349.
2. Fisher S, Genbacev O, Maidji E, Pereira L. Human cytomegalovirus infection of placental cytotrophoblasts in vitro and in utero: implications for transmission and pathogenesis. *J Virol* 2000;74:6808–6820.
3. Kenneson A, Cannon MJ. Review and meta-analysis of the epidemiology of congenital cytomegalovirus (CMV) infection. *Rev Med Virol* 2007;17:253–276.
4. Goderis J, De Leenheer E, Smets K, Van Hoecke H, Keymeulen A, Dhooze I. Hearing loss and congenital CMV infection: a systematic review. *Pediatrics* 2014;134:972–982.
5. Tanaka K, Yamada H, Minami M, Kataoka S, Numazaki K, Minakami H, Tsutsumi H. Screening for vaginal shedding of cytomegalovirus in healthy pregnant women using real-time PCR: correlation of CMV in the vagina and adverse outcome of pregnancy. *J Med Virol* 2006;78:757–759.
6. Dessy E, Corrias A, Nurchi AM, Puxeddu E, Mascia R, Frau G. Congenital hepatic dysplasia from cytomegalovirus. *Pathologica* 1993;85:91–95.
7. Li WW, Shan JJ, Lin LL, Xie T, He LL, Yang Y, Wang SC. Disturbance in plasma metabolic profile in different types of human cytomegalovirus-induced liver injury in infants. *Sci Rep* 2017;7:15696.
8. Bilavsky E, Schwarz M, Bar-Sever Z, Pardo J, Amir J. Hepatic involvement in congenital cytomegalovirus infection - infrequent yet significant. *J Viral Hepat* 2015;22:763–768.
9. Shibata Y, Kitajima N, Kawada J, Sugaya N, Nishikawa K, Morishima T, Kimura H. Association of cytomegalovirus with infantile hepatitis. *Microbiol Immunol* 2005;49:771–777.
10. Goedhals D, Kriel J, Hertzog ML, Janse van Rensburg MN. Human cytomegalovirus infection in infants with prolonged neonatal jaundice. *J Clin Virol* 2008;43:216–218.
11. Dunn W, Chou C, Li H, Hai R, Patterson D, Stolz V, Zhu H, Liu F. Functional profiling of a human cytomegalovirus genome. *Proc Natl Acad Sci U S A* 2003;100:14223–14228.
12. Hermiston TW, Malone CL, Witte PR, Stinski MF. Identification and characterization of the human cytomegalovirus immediate-early region 2 gene that stimulates gene expression from an inducible promoter. *J Virol* 1987;61:3214–3221.
13. Stinski MF, Petrik DT. Functional roles of the human cytomegalovirus essential IE86 protein. *Curr Top Microbiol Immunol* 2008;325:133–152.
14. Han D, Byun SH, Kim J, Kwon M, Pleasure SJ, Ahn JH, Yoon K. Human cytomegalovirus ie2 protein disturbs brain development by the dysregulation of neural stem cell maintenance and the polarization of migrating neurons. *J Virol* 2017;91, e00799–17.
15. Decaens T, Godard C, de Reyniès A, Rickman DS, Tronche F, Couty JP, Perret C, Colnot S. Stabilization of beta-catenin affects mouse embryonic liver growth and hepatoblast fate. *Hepatology* 2008;47:247–258.
16. Harper JW, Adami GR, Wei N, Keyomarsi K, Elledge SJ. The p21 Cdk-interacting protein Cip1 is a potent inhibitor of G1 cyclin-dependent kinases. *Cell* 1993;75:805–816.
17. Toyoshima H, Hunter T. p27, a novel inhibitor of G1 cyclin-Cdk protein kinase activity, is related to p21. *Cell* 1994;78:67–74.
18. Mah LJ, El-Osta A, Karagiannis TC. gammaH2AX: a sensitive molecular marker of DNA damage and repair. *Leukemia* 2010;24:679–686.
19. Fukumitsu K, Ishii T, Yasuchika K, Amagai Y, Kawamura-Saito M, Kawamoto T, Kawase E, Suemori H, Nakatsuji N, Ikai I, Uemoto S. Establishment of a cell line derived from a mouse fetal liver that has the characteristic to promote the hepatic maturation of mouse embryonic stem cells by a coculture method. *Tissue Eng Part A* 2009;15:3847–3856.
20. Darlington GJ, Wang N, Hanson RW. C/EBP alpha: a critical regulator of genes governing integrative metabolic processes. *Curr Opin Genet Dev* 1995;5:565–570.
21. Zannis VI, Kan HY, Kritis A, Zanni E, Kardassis D. Transcriptional regulation of the human apolipoprotein genes. *Front Biosci* 2001;6:D456–D504.
22. Cardot P, Chambaz J, Kardassis D, Cladaras C, Zannis VI. Factors participating in the liver-specific expression of the human apolipoprotein A-II gene and their significance for transcription. *Biochemistry* 1993;32:9080–9093.
23. Niu J, Wang Z, Liu L, Zhang X, Niu D, Liu T, Qiao H, Lu R, Nan F, Tian Z, Wang B. Human cytomegalovirus IE2 may impair the cognitive ability of the hippocampus through the GluNRs/CaMKII α /CREB signaling pathway in the Rosa26-LSL-IE2/Cre mouse. *Behav Brain Res* 2022;419:113683.
24. Yang L, Wang WH, Qiu WL, Guo Z, Bi E, Xu CR. A single-cell transcriptomic analysis reveals precise pathways and regulatory mechanisms underlying hepatoblast differentiation. *Hepatology* 2017;66:1387–1401.
25. Murphy EA, Strebblow DN, Nelson JA, Stinski MF. The human cytomegalovirus IE86 protein can block cell cycle progression after inducing transition into the S phase of permissive cells. *J Virol* 2000;74:7108–7118.
26. Wu H, Wade M, Krall L, Grisham J, Xiong Y, Van Dyke T. Targeted in vivo expression of the cyclin-dependent kinase inhibitor p21 halts hepatocyte cell-cycle

- progression, postnatal liver development and regeneration. *Genes Dev* 1996;10:245–260.
27. Yu Z, Wang Y, Liu L, Zhang X, Jiang S, Wang B. Apoptosis disorder, a key pathogenesis of HCMV-related diseases. *Int J Mol Sci* 2021;22:4106.
 28. Chien H, Dix RD. Evidence for multiple cell death pathways during development of experimental cytomegalovirus retinitis in mice with retrovirus-induced immunosuppression: apoptosis, necroptosis, and pyroptosis. *J Virol* 2012;86:10961–10978.
 29. Chiou SH, Liu JH, Hsu WM, Chen SS, Chang SY, Juan LJ, Lin JC, Yang YT, Wong WW, Liu CY, Lin YS, Liu WT, Wu CW. Up-regulation of Fas ligand expression by human cytomegalovirus immediate-early gene product 2: a novel mechanism in cytomegalovirus-induced apoptosis in human retina. *J Immunol* 2001;167:4098–4103.
 30. Fattuoni C, Palmas F, Noto A, Barberini L, Mussap M, Grapov D, Dessi A, Casu M, Casanova A, Furione M, Arossa A, Spinillo A, Baldanti F, Fanos V, Zavattoni M. Primary HCMV infection in pregnancy from classic data towards metabolomics: an exploratory analysis. *Clin Chim Acta* 2016;460:23–32.
 31. Zhang X, Wang Y, Qian D, Wang Z, Qin Z, Liu X, Liu T, Wang B. HCMV-encoded IE2 promotes NAFLD progression by up-regulation of SREBP1c expression in UL122 genetically modified mice. *Int J Clin Exp Pathol* 2018;11:4213–4220.
 32. Dinić S, Bogojević D, Petrović M, Poznanović G, Ivanović-Matić S, Mihailović M. C/EBP alpha and C/EBP beta regulate haptoglobin gene expression during rat liver development and the acute-phase response. *Mol Biol Rep* 2005;32:141–147.
 33. Parviz F, Matullo C, Garrison WD, Savatski L, Adamson JW, Ning G, Kaestner KH, Rossi JM, Zaret KS, Duncan SA. Hepatocyte nuclear factor 4alpha controls the development of a hepatic epithelium and liver morphogenesis. *Nat Genet* 2003;34:292–296.
 34. Bolger AM, Lohse M, Usadel B. Trimmomatic: a flexible trimmer for Illumina sequence data. *Bioinformatics* 2014;30:2114–2120.
 35. López-Fernández H, Blanco-Míguez A, Fdez-Riverola F, Sánchez B, Lourenço A. DEWE: A novel tool for executing differential expression RNA-Seq workflows in biomedical research. *Comput Biol Med* 2019;107:197–205.
 36. Norton AJ, Jordan S, Yeomans P. Brief, high-temperature heat denaturation (pressure cooking): a simple and effective method of antigen retrieval for routinely processed tissues. *J Pathol* 1994;173:371–379.
 37. Wallberg F, Tenev T, Meier P. Analysis of apoptosis and necroptosis by fluorescence-activated cell sorting. *Cold Spring Harb Protoc* 2016;2016, pdb.prot087387.
 38. Pozarowski P, Darzynkiewicz Z. Analysis of cell cycle by flow cytometry. *Methods Mol Biol* 2004;281:301–311.

Received December 9, 2021. Accepted May 5, 2022.

Correspondence

Address correspondence to: Yunyang Wang, MD, Department of Endocrinology and Metabolism, Affiliated Hospital of Qingdao University, Qingdao, China. e-mail: wangyy_09@outlook.com; fax: (86)-010-63016616; or Bin Wang, PhD, Department of Pathogenic Biology, School of Basic Medicine, Qingdao University, Qingdao, China; fax: (86)-532-85953085 e-mail: wangbin532@126.com.

CRediT Authorship Contributions

Xianjuan Zhang (Conceptualization: Equal; Data curation: Equal; Formal analysis: Equal; Investigation: Equal; Methodology: Equal; Project administration: Equal; Resources: Equal; Software: Equal; Supervision: Equal; Validation: Equal; Visualization: Equal; Writing – original draft: Equal; Writing – review & editing: Equal)

Shasha Jiang (Software: Equal)

Xiaoqiong Zhou (Methodology: Equal)

Zhongjie Yu (Data curation: Equal; Supervision: Equal; Writing – review & editing: Equal)

Shuo Han (Writing – review & editing: Equal)

Fulong Nan (Methodology: Equal; Software: Equal)

Hongye Qiao (Methodology: Equal)

Delei Niu (Methodology: Equal)

Zhifei Wang (Resources: Equal)

Junyun Niu (Software: Equal)

Hong Zhang (Methodology: Equal)

Ting Liu (Software: Equal)

Yunyang Wang (Data curation: Equal; Formal analysis: Equal; Funding acquisition: Supporting; Investigation: Equal; Project administration: Equal; Supervision: Equal; Validation: Equal; Visualization: Equal; Writing – review & editing: Equal)

Bin Wang (Funding acquisition: Lead; Project administration: Lead; Writing – review & editing: Lead)

Conflicts of interest

The authors disclose no conflicts.

Funding

This research was supported by the Shandong Provincial Science and Technology Foundation (2019JZZY011009), Qingdao Municipal Science and Technology Foundation (20-2-3-4-nsh), National Key Research and Development Program of China (2018YFA0900802), Shandong Provincial Natural Science Foundation (ZR2021QH254), and the Qingdao Postdoctoral Application Research Project (RZ2100001326).

Data Availability Statement

The original contributions presented in the study are included in the article/Supplementary Material; further inquiries can be directed to the corresponding authors.